RUSSIAN ACADEMY OF SCIENCES PETERSBURG
NUCLEAR PHYSICS INSTITUTE

A. A. Jgoun, S. I. Manayenkov

Relative yields of K_S^0 in semi-inclusive deep inelastic positron scattering on ^{1}H, ^{2}H nuclei.

Gatchina — 2000

УДК 539.12

Полуинклюзивные относительные выходы K_s^0 в реакции глубоконеупругого рассеяния позитронов на водородной и дейтериевой мишенях.

А.А.Жгун, С.И.Манаенков

Аннотация

С помощью спектрометра HERMES на ускорителе HERA (DESY, Германия) измерялось рождение K_s^0 в глубоконеупругом рассеянии позитронов на нуклонах. Были получены относительные выходы K_s^0 на водородной и дейтериевой мишенях и фрагментационная функция $D_u^{K_s^0}(z)$. Для анализа использовались данные, полученные в 1996-97 годах.

Abstract

HERMES provides the measurements of neutral kaon production in semi-inclusive deep inelastic scattering (SIDIS) of polarized positrons on unpolarized and longitudinally polarized nucleus. The relative yields of K^0_S on ^{1}H, ^{2}H and the fragmentation function $D_u^{K^0_S}(z)$ are obtained. The analysis is based on the data collected with the HERMES detector in years 1996 to 1997.

1 Multi-Dimension Unfolding

Kinematics of the K^0_S-production in SIDIS is determined by six independent variables ($Q^2,\ y,\ \phi,\ z,\ P_\perp,\ \phi^\gamma$). Here $q^2 = -Q^2$ is the squared virtual photon mass and $y = 1 - E'/E_e$, ϕ, z, $P_\perp = |\vec{P}_\perp|$, and ϕ^γ are the fractional energy lost by the lepton, the azimuthal angle of the scattered lepton, the ratio of the energy of a produced hadron h to the photon energy, the transverse momentum of the hadron with respect to the direction of the virtual photon momentum, and the angle between the positron scattering plane and $\vec{P}_\perp$ in the laboratory system, respectively (see Fig. 1). The total energy of the K^0_S meson, E_K is related to the beam energy E_e by the formula

$$E_K = E_e y z. \tag{1}$$

We obtain the K^0_S momentum by measuring the pion momenta in the decay $K^0_S \to \pi^+ + \pi^-$.

Let dN^{true}/dU be the true distribution of the events (measured with an ideal detector) with the $\pi^+\pi^-$ pair originated from the K^0_S decay, where U is a short notation for a set of the true variables $U \equiv (Q^2, y, z, P_\perp, \phi^\gamma)$. The distribution dN^{true}/dU is related with the cross section of the K^0_S-production by the formula

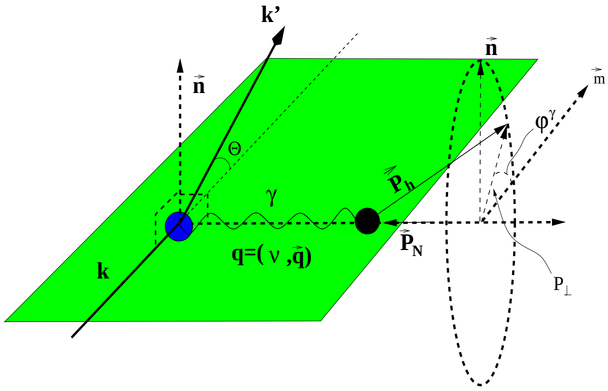

Figure 1: Kinematics of semi-inclusive deep inelastic scattering $e + N \to e'$+h+X. The scattering plane is defined by the lepton momenta $\mathbf{k}$ and $\mathbf{k}'$.

$$\frac{dN^{true}}{dU} = Lw \frac{d\sigma^K}{dQ^2 dy dz dP_\perp d\phi^\gamma} \tag{2}$$

where $dU = dQ^2 dy dz dP_\perp d\phi^\gamma$, L denotes the integrated luminosity and w is the branching ratio of the decay $K_S^0 \to \pi^+ + \pi^-$. Let us denote by V the set of the measured quantities Q^2, y, z, $P_\perp$, ϕ^γ. The values of measured variables V do not coincide with the true values of U due to the finite resolution of the HERMES detector. But the distribution of the reconstructed experimental events dN^{exp}/dV is to be linearly related to the true event distribution dN^{true}/dU, hence we have

$$\frac{dN^{exp}}{dV} = \int A(V,U) \frac{dN^{true}}{dU} dU \tag{3}$$

where the function A describes a detector resolution, acceptance, and reconstruction efficiency. We shall name $A(V,U)$ the detector function. The probability to register the scattered positron trajectory and the secondary particles depends not only on the variables, which have been mentioned above, but it depends also on other variables (the azimuthal angle of the scattered positron ϕ, the point of the positron interaction with the target, a length of K_S^0 trajectory, values of pion momenta in the kaon decay etc.). It is assumed that $A(V,U)$ is the result of integration over all variables except V and U.

To find the true event distribution dN^{true}/dU one needs the experimentally measured distribution dN^{exp}/dV and detector function $A(V,U)$ and has to solve (3) which is the Fredholm integral equation of the first kind. The most important property of integral equation (3) is the factorization property: the kernel $A(V,U)$ depends on the detector resolution, acceptance, and reconstruction efficiency but does not depend on the studied distribution dN^{true}/dU (the form of the cross section). Vice versa the quantity of interest dN^{true}/dU does not depend on the detector properties. This factorization permits to get the detector function with the aid of the Monte Carlo simulations even if the initial distribution dN^{in}/dU applied in the MC programs (the generator for the cross section) deviates significantly from the true distribution dN^{true}/dU (the physical cross section). The minimal number of the used variables is equal to the number of variables on which the cross section depends. For the case under discussion, this number is equal to five ($Q^2,\ y,\ z,\ P_\perp,\ \phi^\gamma$) since the cross section does not depend on ϕ.

Integrating (3) over all variables except one (say z) and applying the Caushy theorem we can get the integral equation of the same type as (3)

$$\frac{dN^{exp}}{dz^{exp}} = \int K(z^{exp}, z^{true}) \frac{dN^{true}}{dz^{true}} dz^{true} \tag{4}$$

but the kernel $K(z^{exp}, z^{true})$ will be dependent both of the detector properties and the form of the multi-dimensional distribution dN^{true}/dU. If the kernel $K(z^{exp}, z^{true})$ is obtained in the MC simulation it depends on the applied generators for the studied process and hence the obtained distribution dN^{true}/dz^{true} can, generally speaking, be different from the real physical quantity. Hence to get the real physical quantities one has to perform the 5-dimensional unfolding. Due to a poor experimental statistics we have to integrate in (3) over ϕ^γ assuming that the cross section as a function of ϕ^γ is very smooth and does not deviates significantly from a constant (in the quark parton model the cross section does not depend on ϕ^γ). We have estimated the systematic uncertainty due to the integration over ϕ^γ.

If we decompose the full kinematic region of the variables U and V into n bins ΔU_j and ΔV_l ($j,\ l = 1,\ ...,\ n$), then integrating (3) over V in the $j-$th bin, we get for $j = 1,\ ...,\ n$

$$\Delta N_j^{exp} = \sum_{l=1}^{n} A_{jl} \Delta N_l^{true} \tag{5}$$

where we have the detector matrix describing the detector resolution, acceptance, and reconstruction efficiency instead of the detector function. Multiplying (5) by the inverse matrix A^{-1} and taking into account (2) one can get the expression for the cross section integrated over the $j-$th bin

$$\Delta\sigma_j = \int\limits_{\Delta U_j} \frac{d\sigma^K}{dQ^2 dy dz dP_\perp d\phi^\gamma} dU = \frac{1}{Lw} \sum_{l=1}^{n} (A^{-1})_{jl} \Delta N_l^{exp}. \tag{6}$$

The formal solution (6) of the matrix equation (5) can have rather large unphysical oscillations of the cross section if the detector matrix is not diagonal and has large dimension $n \times n$. The oscillations under discussion are due to the unstability of the solution of (5) with respect to the small variations of ΔN_l^{exp}. The statistical uncertainties of the measured distribution ΔN_l^{exp} play the role of these variations. Besides the detector matrix is obtained through the MC simulation and also has statistical uncertainties being the origin of the oscillations. That is why the matrix inverse method has to be impoved. We have used two improved methods of the matrix inversion:

• – parameter estimation method [1];
• – unfolding method based on the Bayes theorem [2]
which suppress the unphysical oscillations and provide smooth cross sections.

2 Event selection

The cuts applied for event selection are given in Table 1. The notations in Table 1 are as follows: W denotes the mass of produced hadrons, E_{calo} is the positron energy measured with the calorimeter, X, Y, Z denote coordinates of the primary DIS vertex with the Z-axis chosen parallel to the beam direction. We have selected events with three and more number of tracks only one of which being identified as the positron track.

Assuming that two other particles with electric charges of opposite signs are pions we choose events with the mass of the $\pi^+\pi^-$-system $M_{\pi\pi}$ in the range $0.475 < M_{\pi\pi} < 0.525$ GeV as candidates for K_S^0-production events with E_K denoting the kaon energy.

The angle β in Table 1 is the angle between the three-momentum of K_S^0 ($\vec{p}$) and the vector $\vec{l}_K$ connecting the DIS vertex with the kaon decay vertex. The K_S^0 lifetime τ has been calculated with the aid of the relation

$$\tau = \frac{M_{\pi\pi}(\vec{l}_K \cdot \vec{p})}{p^2} \ . \tag{7}$$

The applied $c\tau$-cut is presented in Table 1 too. Owing to the misidentification the other two particles (other than the positron) can be the e^+e^- or π^-p ($\pi^+\bar{p}$) system, but not two pions. To remove such events the cuts for the masses M_{ee} and $M_{\pi p}$ have been applied (see Table 1).

After event selection we have accumulated ∼9600 candidates for

Table 1: Track and event selection

All tracks		
Quantity	Range	Unit
Fidicial cuts	Yes	
Momentum	$\geq$0.3	GeV/c
Positron tracks		
Q^2	$\geq$0.8	$(GeV/c)^2$
W^2	$\geq$4	$(GeV)^2$
E_{calo}	$\geq$3.5	GeV
y	[0.28,0.85]	
x	[0.017,1]	
Z coordinate of primary vertex	[-20,20]	cm
$\sqrt{X^2+Y^2}$ of primary vertex	[0,0.75]	cm
K_s^0 candidate selection		
M_{ee}	> 0.13	GeV
$M_{p\pi}$	< 1.11 or > 1.123	GeV
$c\tau$	> 0.5	cm
$\cos\beta$	> 0.995	
$M_{\pi\pi}$	[0.475,0.525]	GeV
E_k/E_{beam}	[0.08,0.50]	

Table 2: Integral yields

Year	1996		1997	
Target	H	D	H	D
$N^{K_s^0}$	1946	2162	2940	2576

the hydrogen and deuterium targets (see Table 2).

The obtained K_s^0 mass resolution (1 standard deviation) is 6 MeV (see Fig. 2 (left)), and we get for the mass of K_s^0 the value 497.70±0.06 MeV compared with the published value of 497.672±0.031 MeV [6]. Such a comparison serves as a check of the HERMES momentum calibration. Let us denote by N_C a number of events in the central region of the $\pi^+\pi^-$ invariant mass distribution ($0.475 < M_{\pi\pi} < 0.525$ GeV) and let N_B be a number of the background events under the K_s^0 peak which we define as

$$N_B = (N_{right} + N_{left})/2 \ . \tag{8}$$

Here N_{left} and N_{right} are numbers of events in the invariant mass regions $0.425 < M_{\pi\pi} < 0.475$ GeV and $0.525 < M_{\pi\pi} < 0.575$ GeV, respectively.

Figure 2 (right) shows the proper lifetime distribution for the observed events N_C (closed circles) and N_B (squares). For a fit of the $c\tau$-distribution we have used the function

$$f(c\tau) = a_1 \exp\left(-a_2 (c\tau)^{0.3}\right) + a_3 \exp\left(-\frac{c\tau}{a_4}\right) \tag{9}$$

both for N_C and N_B. The first term in formula (9) describes the background events and the second term corresponds to the real K_S^0-events. The two terms in (9) are nonzero both for N_C and N_B but the ratio a_3/a_1 for the central region is essentially larger than for N_B. A nonzero value of a_3 in the $c\tau$-distribution of the N_B-events means that the K_S^0-mass distribution is not Gaussian-like and there is an appreciable number of real K_S^0-events among N_B-events (beyond the $\pm 4\sigma$-region in the mass distribution). Using values of obtained parameters a_1 - a_4 it is possible to find the real number of the K_S^0-events both among N_C and N_B. The mean value of $c\tau$ for K_S^0 (the fit parameter a_4) is found to be 2.70 ±0.03 cm in good agreement with the expected value 2.6762±0.0024 [6].

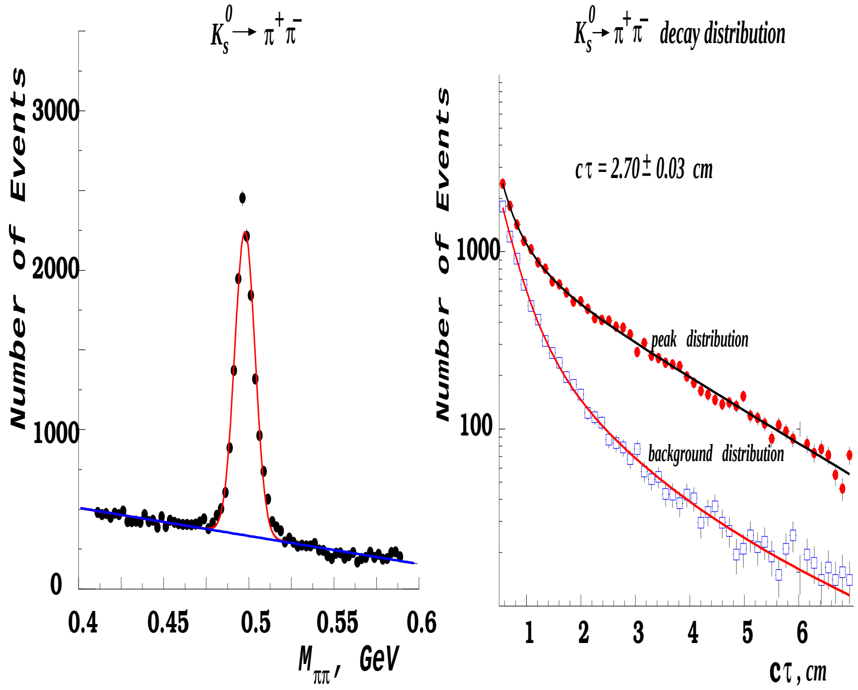

Figure 2: Invariant mass distribution of $\pi^+\pi^-$-system (left) and $c\tau$ distribution (right). Closed circles (right) show $c\tau$-distribution in region of K_S^0-peak ($0.475 < M_{\pi\pi} < 0.525$ GeV), squares present distribution for background events. Applied cuts are given in Table 1 and for definition of background see (8).

3 Comparison with Monte Carlo calculation

Monte Carlo analysis is based on the Hermes Monte Carlo program HMC(84b8) with default parameters and the Hermes Reconstruction program HRC(96.011). The hits from the vertex chambers have not used in the present analysis.

The 1996-97 data contain $\sim$ 9600 K_s^0 events. We have used for the present analysis the data on the polarized proton combining the data with opposite target polarization in such a way to have the mean value of the target polarization equal to zero. We have added these data to the data on the unpolarized targets analysed in our previous report [4]. 180K Monte Carlo semi-inclusive K_s^0 events have been reconstructed with the same conditions as for the data. Both the experimental and Monte Carlo distributions are normalized to the unity. Results of the comparison of the experimental event distributions on the hydrogen with the Monte Carlo calculations are presented in Fig. 3 ($\Delta n_j^{exp}/\Delta n_j^{MC}$). One can see that the Monte Carlo distributions for all presented variables disagree with the experimental data (y-distribution: $\chi^2/N_{d.f.} = 12.56$, Q^2-distribution: $\chi^2/N_{d.f.} = 1.41$, $P_\perp^2$-distribution: $\chi^2/N_{d.f.} = 11.24$, z-distribution: $\chi^2/N_{d.f.} = 14.50$). It is easy to see that the shapes of the Monte Carlo and experimental distributions are different. We come to the conclusion that in obtaining the cross sections of semi-inclusive scattering and asymmetries we are to apply methods which do not depend (at least crucially) on the shapes of MC distributions. On the other hand the discrepancy under consideration means that the HERMES data contain new information about the K_S^0-production in SIDIS which is complimentary to the information accumulated in the applied Monte Carlo programs.

4 Test of method

To test how the applied unfolding procedure restores the initial distribution dN^{true}/dU, we have used two different MC distributions.

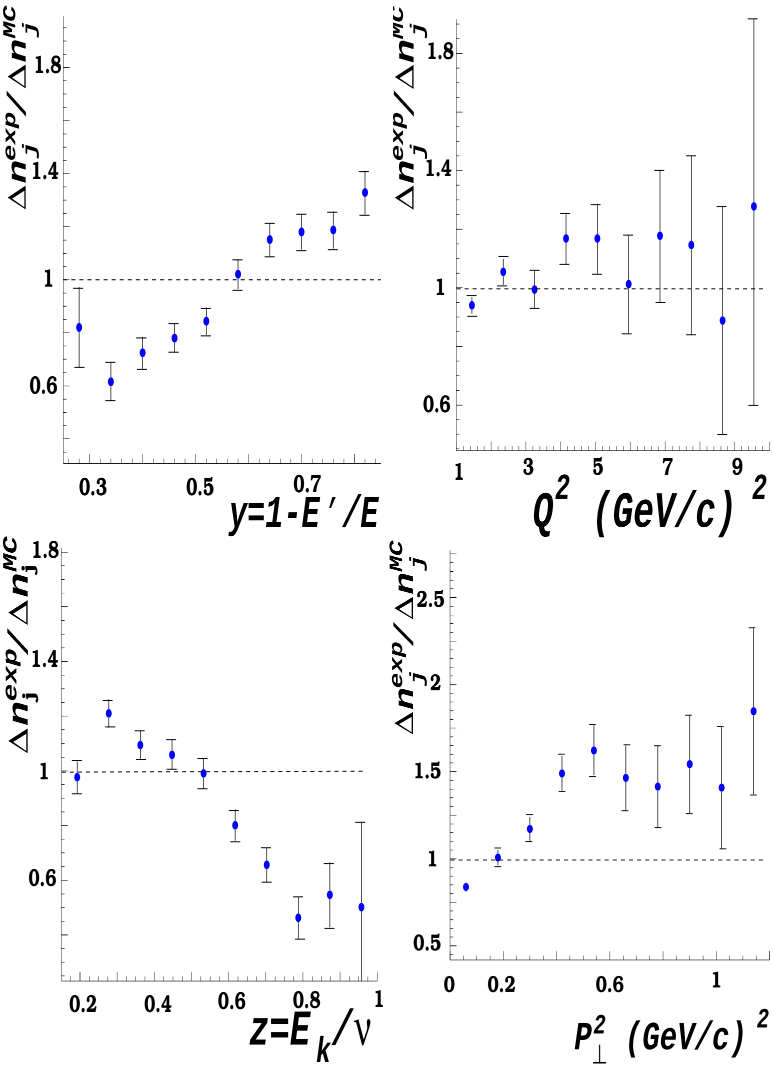

Figure 3: Ratios of experimental kinematic distributions and Monte Carlo distributions for kinematic variables of semi-inclusive reaction.

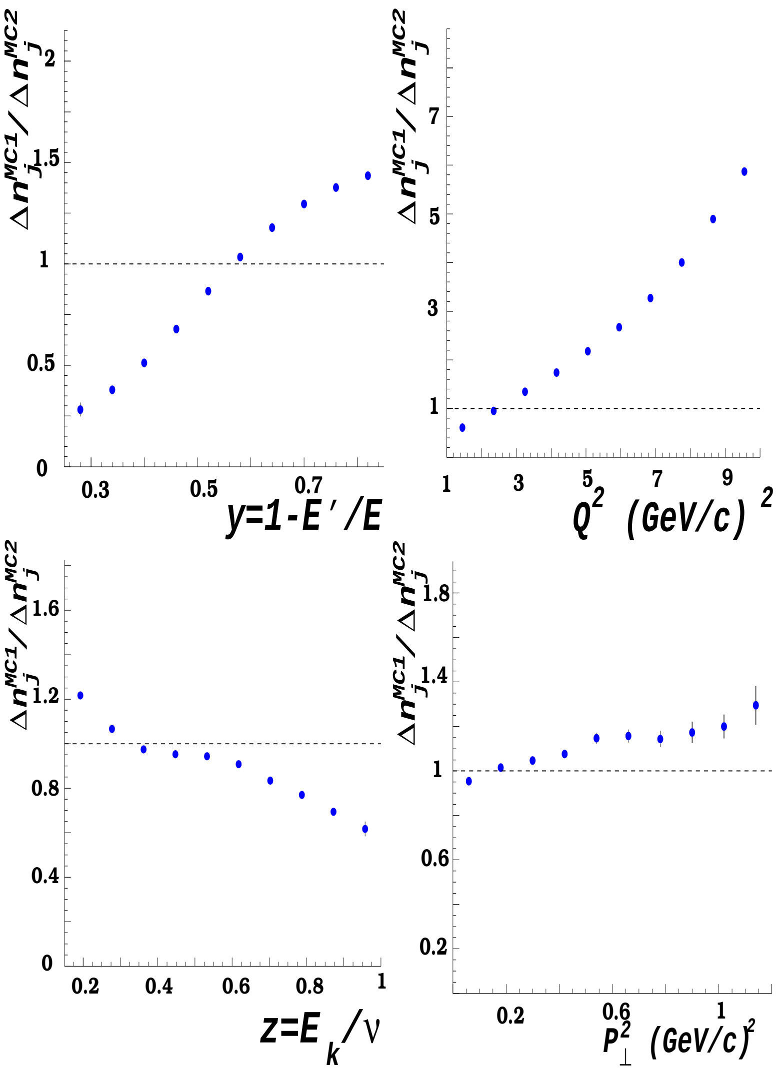

Figure 4: Ratios of "experimental" (Δn_j^{MC1}) and Monte Carlo event number (Δn_j^{MC2}) in j-th bin for distributions normalized to unity.

The former distribution dN^{MC1}/dU is considered as the experimental data. The latter distribution dN^{MC2}/dU plays the role of the MC distribution applied to find the detector matrix A_{jl}. The obtained distribution dN^{MC2}/dU is very different from dN^{MC1}/dU as one can see from Fig. 4 where we present the ratio of these distributions normalized to the unity $(\Delta n_j^{MC1}/\Delta n_j^{MC2})$. Choosing different binning with a number of y-bins equal to 1, 4, 10 (the number of bins for z and $P_\perp^2$ is equal to 1) we have calculated the quantity $(\Delta N_j^{MC1} - \Delta N_j^{unf})/\Delta N_j^{MC1}$ which describes the efficiency of the unfolding procedure. Here ΔN_j^{MC1} denotes a number of the "experimental" events in the $j-$th bin and ΔN_j^{unf} is the number of events obtained after the unfolding procedure.

Figure 5 (left) shows a comparison of the initial "experimental" distribution with the unfolded distribution. We get $\chi^2/N_{d.f.} = 202.6$ for one-dimensional unfolding $(N_y = 1)$, $\chi^2/N_{d.f.} = 17.08$ for two-dimensional unfolding with 4 bins for the y-distribution, $\chi^2/N_{d.f.} = 8.82$ for two-dimensional unfolding with 10 bins for the y-distribution. For 4-dimensional unfolding with $N_{Q^2} = 10$, $N_y = 10$, $N_z = 5$, $N_{P_\perp^2} = 5$, we have $\chi^2/N_{d.f.} = 0.22$. We see that 1-dimensional unfolding does not permit to restore the initial distribution. The 2-dimensional unfolding for the variables Q^2 and y provides a better result than the 1-dimensional one. But the result is not satisfactory even though the difference of the two MC distributions for variables z and $P_\perp^2$ is not as crucial as for Q^2 and y (compare the top and bottom parts of Fig. 4). The 4-dimensional unfolding gives a better value of $\chi^2/N_{d.f.}$ than the 2-dimensional one since it takes better into account the smearing effects for all four variables.

Bins should be chosen so that the obtained cross section would be independent of binning which means that the systematic errors related to the bin number are smaller than the statistical ones. If the range of every bin goes to zero and the number of MC events per bin goes to infinity, then the obtained efficiency does not depend

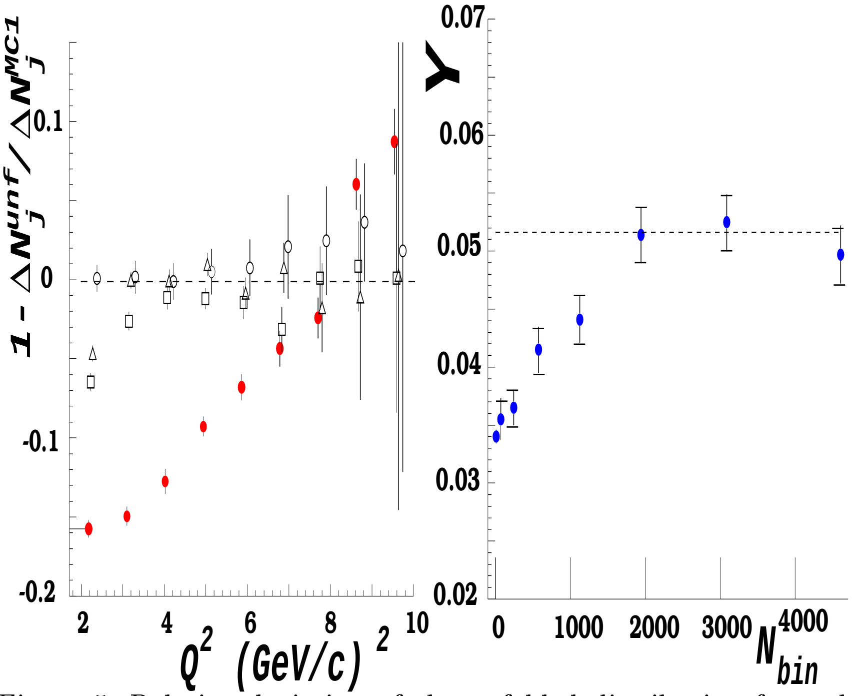

Figure 5: Relative deviation of the unfolded distribution from the initial distribution for different number of bins (left). • - one dimesional unfolding, □ - two dimensional unfolding (40 bins), △ - two dimensional unfolding (100 bins), ∘ - four dimensional unfolding. Optimization of binning for four dimensional unfolding of total yield Y (right). Points show dependence of Y on total number of bins $N_{bin} = N_{Q^2} N_y N_z N_{P_\perp^2}$.

on the theoretical model for the cross section of the semi-inclusive K_S^0-production used in the MC program as it has been discussed above. Figure 5 (right) shows total experimental yields for different number of bins. Bearing in mind to get 9 experimental points for the z-dependence of the yield we put $N_z = 9$ and do not change this number. After that we calculate the yield for the numbers of bins $N_{Q^2} = N_y = N_{P_\perp^2} = m$ with $m = 1, 2, 3, 4, 5, 6, 7, 8$. Figure 5 (right) shows the total yield versus N_{bin}, where $N_{bin} = N_z N_{Q^2} N_y N_{P_\perp^2}$ denotes a total number of bins. One can see that results become stable for the 4-dimensional unfolding with $m \geq 6$. We would like to remark that for different variables the stable result of the unfolding procedure starts from different numbers of bin. For example, the minimal value of N_{Q^2} is equal to 5.

It is possible to get the detector matrix for the region $0.5 < Q^2 < 10$ (GeV/c)^2, $0.20 < y < 0.9$, $0.1 < z < 1$, $P_\perp^2 < 2$ (GeV/c)^2 only since the HERMES detector function obtained through the MC simulation out of these regions is very small. We have chosen the following binning for extraction of the experimental cross section:

$Q^2,\ (GeV/c)^2$:	0.8; 1; 1.5; 2; 4; 10
y :	0.28; 0.42; 0.54; 0.64; 0.73; 0.8; 0.85
z :	0.15; 0.25; 0.34; 0.43; 0.52; 0.61; 0.7; 0.8; 0.9; 1
$P_\perp^2,\ (GeV/c)^2$:	0.; 0.02; 0.05; 0.09; 0.25; 0.49; 0.81; 2.0

5 Systematic errors

The systematic uncertainty of the relative yield includes the systematic error of the unfolding method, the systematic error due to the applied cuts, and the uncertainty due to the ϕ^γ-dependence both of the cross section and the detector efficiency.

The accumulated number of the MC events (180000) used for obtaining the detector matrix is more than ten times greater the number of experimental events. Hence the contribution of the statistical errors due to uncertainties of the detector matrix to the total statistical uncertainty is practically negligible compared with the contribution of the statistical errors of the data.

Cuts have been chosen as a result of minimization procedure of the fractional statistic uncertainty of the total yield Y given by the relation

$$\frac{\delta Y}{Y} = \frac{1}{\sqrt{N_C}} \frac{\sqrt{1 + N_B/N_C}}{1 - N_B/N_C}. \tag{10}$$

The results of the minimization presented in Fig. 6 show that the

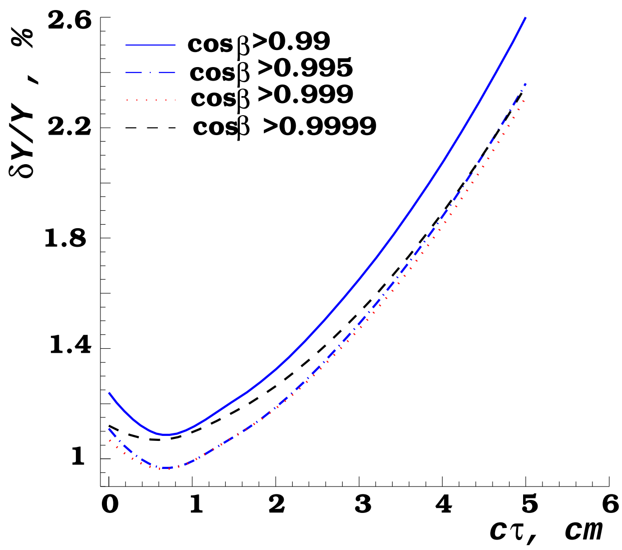

Figure 6: Minimization of fractional statistical error of total yield of K_s^0 in semi–inclusive deep inelastic ep scattering.

optimal value for $c\tau$ is between 0.5 and 0.7 cm. We see also from Fig. 6 that $\delta Y/Y$ changes not more than by a factor 1.15 for $0.99 < \cos\beta < 0.9995$ at the optimal value of $c\tau$ which means that all values of $\cos\beta$ in the range under discussion are admissible. We remind that the angle β is the angle between the three-momentum of K_S^0 and the vector $\vec{l}_K$ connecting the DIS vertex with the kaon decay vertex and τ is defined with (7).

We have studied the dependence of the cross section of the K_S^0-production in SIDIS on the applied geometrical cuts. Let us define the ratio K^{exp} of the number of the experimental events with some cut N^{cut} to the initial event number N^{in} (without the cut) and let K^{MC} denotes the same ratio for the MC events. If the applied MC programs describe the detector efficiency, resolution and acceptance perfectly then $K^{exp} = K^{MC}$ otherwise we can consider the ratio

$$R^{cut} = \frac{K^{MC}}{K^{exp}} \tag{11}$$

whose deviation from the unity will be a measure of the fractional systematic uncertainty due to an application of the cut. Figure 7 (right) illustrates a dependence of R^{cut} defined by (11) on the collinearity cut. We see that for the hard collinearity cut $\cos\beta > 0.9995$ the ratio deviates from the unity by 12% which is an estimate of the systematic uncertainty due to the applied cut. The dependence of R^{cut} on the $c\tau$-cut is presented in the left part of Fig. 7. To decrease a value of the systematic error due to application of the geometrical cuts we make use of the softer cuts than those applied in [3] and [4]. We have studied an influence of a sum of different cuts to the ratio R^{cut}. For the first set of cuts $M_{ee} > 0.13$ GeV, $c\tau > 0.5$ cm and $\cos\beta > 0.995$ the ratio is equal to 1.03. For the second set of cuts $M_{ee} > 0.13$ GeV, $c\tau > 0.7$ cm and $\cos\beta > 0.999$ $R^{cut} = 1.06$ and for the hard cuts $|\vec{l}_K| > 10$ cm, $\cos\beta > 0.9995$ the ratio is equal to 1.13. We see that an application of hard geometrical cuts makes systematic uncertainties comparable (and sometimes even larger) with the statistical errors. In the present work, we have used the cuts $M_{ee} > 0.13$ GeV, $c\tau > 0.5$ cm, $\cos\beta > 0.995$ and we estimate the systematic uncertainty related with the geometrical cuts to be 3%. The hard

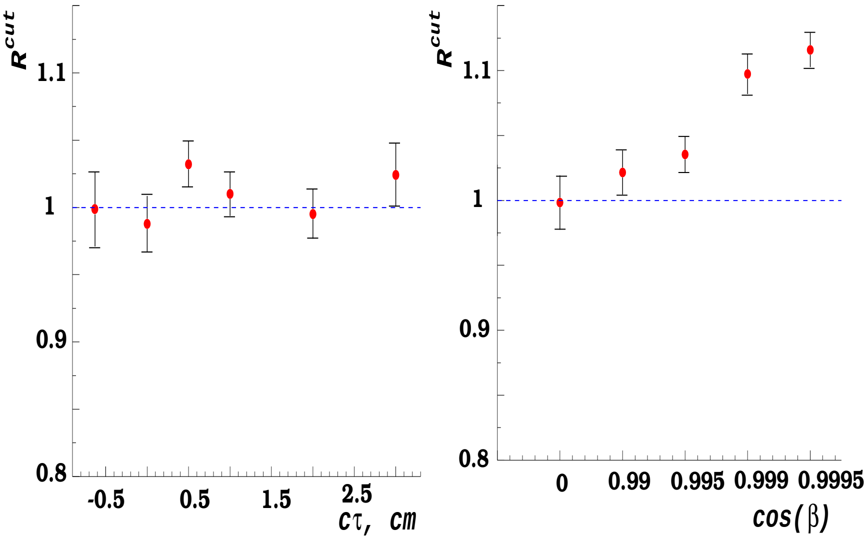

Figure 7: Dependence of R^{cut} on $c\tau$-cut (left) and on collinearity cut (right). Ratio R^{cut} is defined in (11).

geometrical cuts permit to suppress the background significantly [3] (down to the level of a few per cents). The cuts used in the present work make the signal background ratio equal approximately to 2:1 (see left part of Fig. 2). One can see from Fig. 2 that the signal of the K_S^0 is unambiguously seen in the mass distribution of the $\pi^+\pi^-$-pairs. Though an application of the softer geometrical cuts increases the statistical errors of the obtained cross sections but permits to have the systematic uncertainty lower than the statistical one.

The number of unfolded events N_j^{Ag} in the j-th bin obtained with the Bayes theorem unfolding method [2] is compared in Fig. 8 with the number of unfolded events N_j^{Bl} found with the method proposed in [1]. The ratio

$$(N_j^{Ag} - N_j^{Bl})/\sqrt{(\delta N_j^{Ag})^2 + (\delta N_j^{Bl})^2}$$

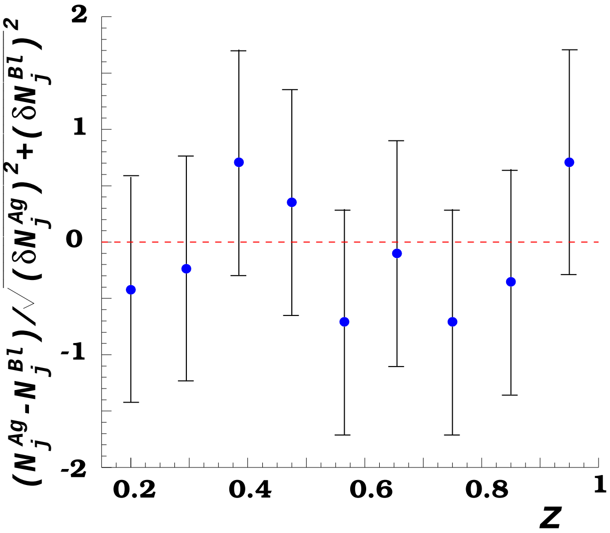

Figure 8: Comparison of unfolding method [2] with method [1]

is shown by circles where δN_j^{Ag} and δN_j^{Bl} denote statistical uncertainties of N_j^{Ag} and N_j^{Bl}, respectively. We can see the results to be in an excellent agreement (within one standard deviation).

The dependence of the cross section on the azimuthal angle ϕ^γ for the semi-inclusive K_S^0-production on unpolarized targets looks like

$$\sigma \sim \sigma_0[1 + R_1 \cos(\phi^\gamma) + R_2 \cos(2\phi^\gamma) + P_B R_3 \sin(\phi^\gamma)] \, . \qquad (12)$$

Formula (12) follows from the Lorentz covariance and parity conservation applied to the hadronic tensor. The third coefficient in the brackets in (12) is proportional to the beam polarization (P_B). If the detector function does not depend on ϕ^γ the sum over all ϕ^γ of the observed number of events is proportional to σ_0 which is the cross section integrated over ϕ^γ with the limits 0 and 2π. If the detector function depends on ϕ^γ and its dependence is described by the formula

$$A(\phi^\gamma) \sim 1 + \sum_{n=1}^{\infty} [a_n \cos(n\phi^\gamma) + b_n \sin(n\phi^\gamma)] \, , \qquad (13)$$

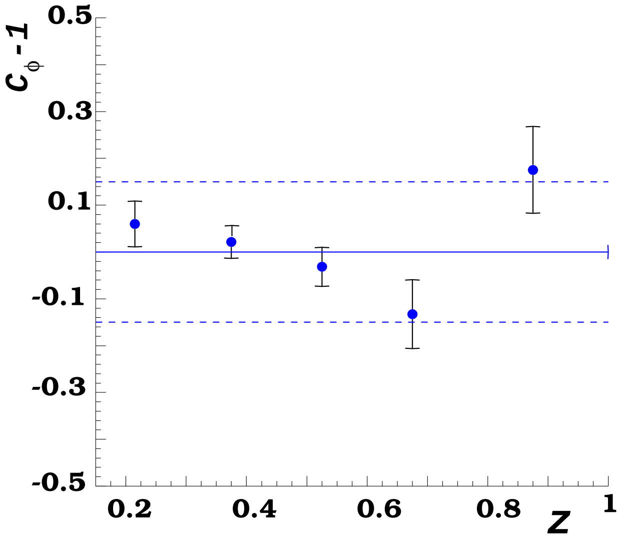

Figure 9: Systematic uncertainty due to ϕ^γ-dependence of detector function and cross section of K^0_S-production in SIDIS. See definition of C_ϕ in (14).

---

then the observed number of events contains the correction factor C_ϕ which is equal to

$$C_\phi = 1 + (a_1 R_1 + a_2 R_2 + P_B b_1 R_3)/2 \; . \qquad (14)$$

To obtain the cross section integrated over all the azimuthal angles (σ_0) one is to divide the observed number of events by C_ϕ. We have considered the cross section averaged over the sign of the beam polarization. For this case the third term in the brackets in (14) cancels. Since C_ϕ has rather large statistical errors (see Fig. 9) we consider a value of $C_\phi - 1$ as a measure of the systematic uncertainty which appears if both the cross section and the detector function depend on ϕ^γ. We have estimated the correction under discussion to be equal to 10 -15%.

All the discussed systematic uncertainties of the relative yields

Table 3: Normalized $z-$distributions $(1/N^{inc})(\Delta N^k/\Delta z)10^2$ for K_S^0-production in SIDIS. The radiation corrections are taken into account in third and fifth columns only.

z	^{1}H		^{2}H	
0.2	$25^{\pm 4}_{\pm 4}$	$31^{\pm 5}_{\pm 5}$	$20^{\pm 4}_{\pm 3}$	$24^{\pm 4}_{\pm 4}$
0.29	$17^{\pm 1}_{\pm 3}$	$21^{\pm 1}_{\pm 3}$	$24^{\pm 2}_{\pm 4}$	$29^{\pm 3}_{\pm 5}$
0.38	$12.6^{\pm 0.6}_{\pm 2}$	$15.6^{\pm 0.7}_{\pm 2}$	$15.3^{\pm 0.7}_{\pm 2}$	$18.6^{\pm 0.9}_{\pm 3}$
0.47	$8.2^{\pm 0.5}_{\pm 1}$	$10.1^{\pm 0.6}_{\pm 2}$	$9.7^{\pm 0.6}_{\pm 1}$	$11.7^{\pm 0.8}_{\pm 2}$
0.56	$4.8^{\pm 0.3}_{\pm 0.7}$	$5.9^{\pm 0.4}_{\pm 0.9}$	$5.5^{\pm 0.6}_{\pm 0.8}$	$67^{\pm 0.7}_{\pm 1}$
0.65	$2.6^{\pm 0.2}_{\pm 0.4}$	$3.2^{\pm 0.2}_{\pm 0.5}$	$2.7^{\pm 0.2}_{\pm 0.4}$	$3.3^{\pm 0.2}_{\pm 0.5}$
0.75	$1.3^{\pm 0.1}_{\pm 0.2}$	$1.7^{\pm 0.2}_{\pm 0.3}$	$1.8^{\pm 0.2}_{\pm 0.3}$	$2.2^{\pm 0.2}_{\pm 0.3}$
0.85	$0.44^{\pm 0.07}_{\pm 0.07}$	$0.54^{\pm 0.09}_{\pm 0.09}$	$0.5^{\pm 0.1}_{\pm 0.1}$	$0.6^{\pm 0.1}_{\pm 0.1}$
0.95	$0.11^{\pm 0.07}_{\pm 0.02}$	$0.13^{\pm 0.09}_{\pm 0.02}$	$0.3^{\pm 0.2}_{\pm 0.4}$	$0.3^{\pm 0.2}_{\pm 0.05}$

have been added in quadrature and presented in Figures. The most important systematic error among them is the systematic uncertainty due to the ϕ^γ-dependence both of the detector efficiency and the cross section of the K_S^0-production in SIDIS.

6 Experimental yields of K_S^0 on ^1H and ^2H

Our final results on the relative yields of K_S^0 (with respect to the total DIS event number N^{inc}) are presented in Tables 3 and 4.

Comparison of the HERMES data with the EMC [7], Cornell university group [8], and FNAL [9] data is presented in Fig. 10 all the data being shown without any radiation corrections. The shadowed band in the bottom part of the Figure shows the fractional systematic uncertainty. One can see that the statistical and systematic uncertainties of the HERMES relative yields are smaller than those obtained

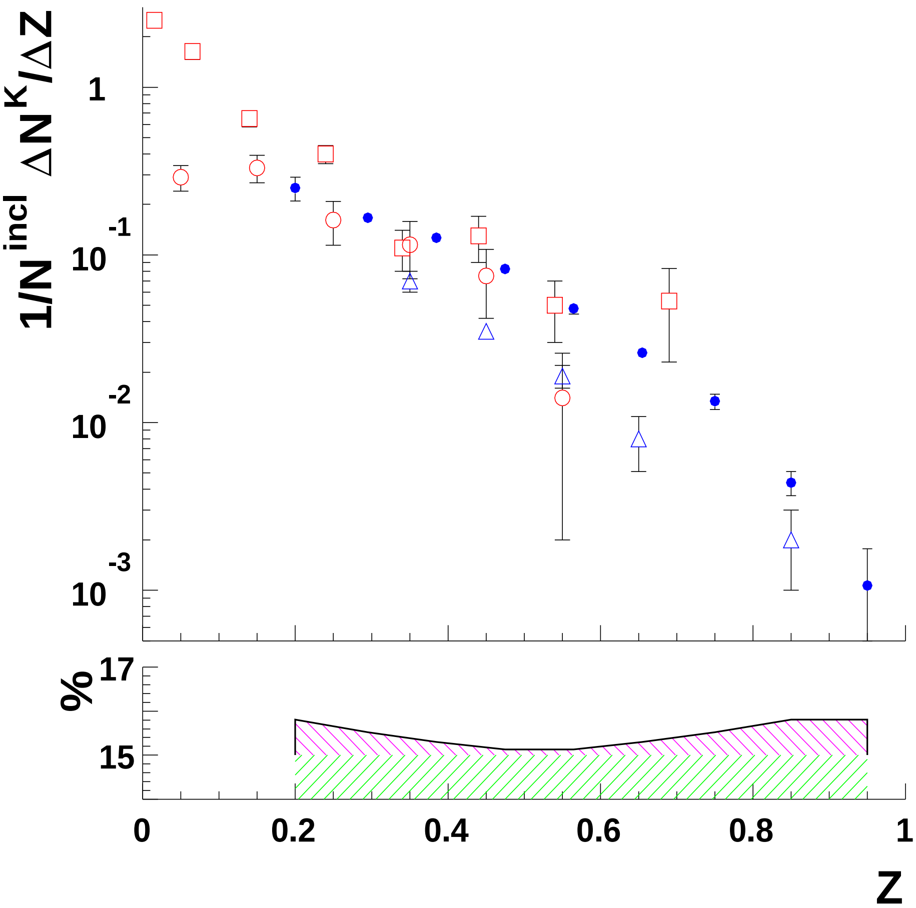

Figure 10: Experimental relative yields of K_S^0 on proton versus z. Experimental data : $\bullet$ - HERMES ($Q^2 > 1$ (GeV/c)^2), $\circ$ - FNAL-398 ($\mu + p$, p_{lab}=225 GeV/c) [9], $\square$ - EMC ($\mu + p$, p_{lab}=280 GeV/c) [7], $\triangle$ - Cornell Univ. ($e + p$, p_{lab}=11.5 Gev/c) [8]. Shaded area in down part of Figure shows fractional systematic errors.

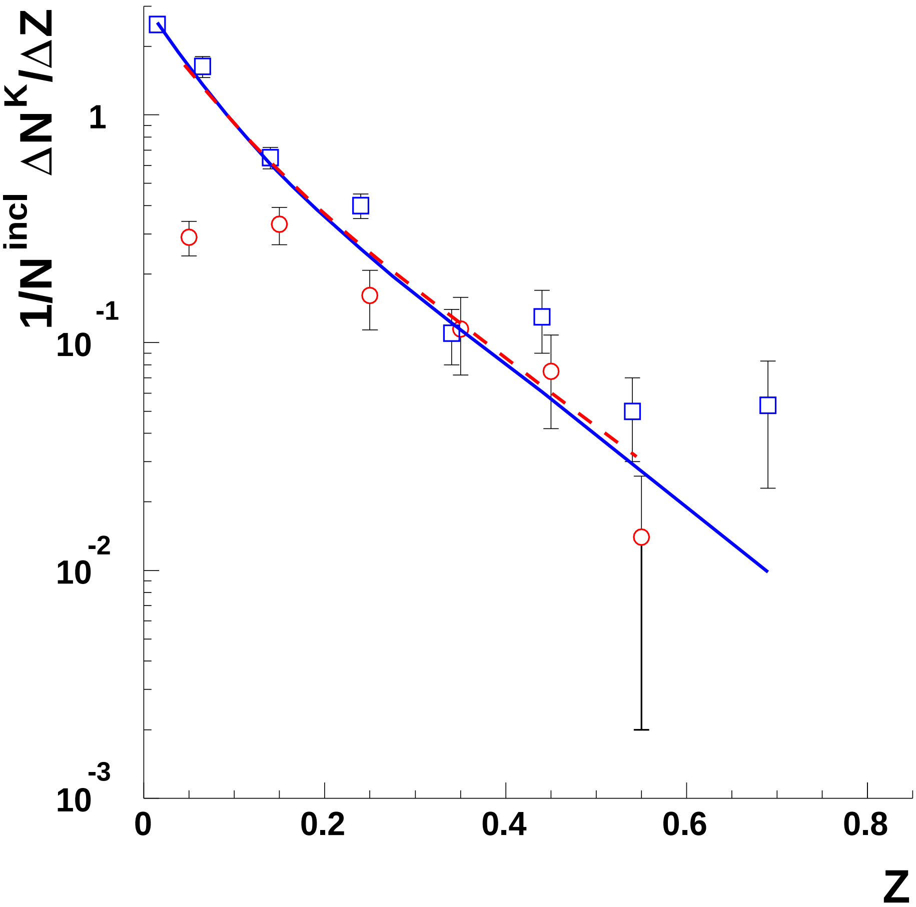

Figure 11: Comparison of relative yields of K_S^0 on proton with Monte Carlo calculations. Experimental data : $\circ$ - FNAL-398 (μ+p, p_{lab}=225 GeV/c) [9], $\square$ - EMC ($\mu + p$, p_{lab}=280 GeV/c) [7]. Solid and dashed histograms - MC calculations with default parameters at p_{lab}=280 GeV/c and p_{lab}=225 GeV/c, respectively.

Table 4: Normalized $P_\perp^2$-distributions ($P_\perp$ in GeV/c) $(1/N^{inc})(\Delta N^k/\Delta P_\perp^2)10^2$ for K_S^0-production in SIDIS. The radiation corrections are taken into account in third and fifth columns only.

$< P_\perp^2 >$	^{1}H		^{2}H	
0.01	26 ± 1	32 ± 2	30 ± 3	36 ± 3
0.035	25 ± 1	31 ± 2	30 ± 2	36 ± 3
0.07	25 ± 2	31 ± 4	29 ± 5	35 ± 5
0.17	9.8 ± 0.8	12 ± 1	11.7 ± 0.8	14 ± 1
0.37	7.0 ± 0.5	8.6 ± 0.7	7.9 ± 0.9	9.6 ± 1
0.65	2.5 ± 0.5	3.1 ± 0.5	1.8 ± 0.2	2.3 ± 0.3
1.40	0.22 ± 0.03	0.27 ± 0.04	0.29 ± 0.05	0.35 ± 0.06

in [7], [8], [9].

To compare the data obtained at different energies, Q^2- and x-regions we have used the MC simulation which permits to take into account the Q^2-evolution. One can see from Fig. 11 that the MC simulation performed with the default parameters is in a good agreement with the EMC data ($\chi^2/N_{d.f.} = 2.17$) ($Q^2 > 4$ (GeV/c)^2) the radiation corrections being taken into account in the MC calculation with the aid of the POLRAD2 program [10]. For more reliable comparison of the FNAL and EMC data, we have used the FNAL data at $Q^2 > 2$ (GeV/c)^2 only since the perturbative QCD evolution equation can be nonapplicable for the low-Q^2 FNAL data ($Q^2 > 0.4$ (GeV/c)^2). We see from Fig. 11 that the difference between two MC calculations is very small hence the dependence of yields on Q^2 and beam energy cannot explain a very serious discrepancy between the EMC and FNAL data at $z < 0.3$ ($\chi^2/N_{d.f.} = 128.2$). The two experiments are in a reasonable agreement at large z (> 0.3). The Cornell university group data disagree with the MC calculation done with the default parameters as it can be seen from Fig. 12 ($\chi^2/N_{d.f.} = 31.62$). The Cornell university group tuned the MC parameters to describe the total yield of K_S^0. One can see that the discrepancy between the MC simulation with the tuned parameters and the Cornell university group data is less than for the MC calculation with the default parameters. But one can see that the MC programs with the tuned parameters do not describe well the experimental z-distribution obtained in [8] ($\chi^2/N_{d.f.} = 6.17$). The radiation corrections have been taken into considerations in the MC calculations both with the default parameters and parameters found in [8]. A word of caution is in order. One should remember that the data [8] have been obtained at rather low Q^2 ($0.5 < Q^2 < 6$ (GeV/c)^2) where an applicability of perturbative QCD is questionable. Hence the disagreement between the data [8] and the MC calculation done within the framework of perturbative QCD may not probably mean a serious discrepancy between the EMC data and the data [8]. The MC calculation performed with the Cornell parameters disagree with the HERMES data as one can see from Fig. 13. This means presumably that the HERMES data are in a contradiction with the Cornell university group data. We can see also that the MC calculation performed with the default parameters describes well the HERMES data at $z > 0.5$. The radiation corrections have been taken into account for the HERMES data but not for the theoretical calculations. Though $\chi^2/N_{d.f.}$ is rather large for $z < 0.5$ (since the statistical accuracy of the HERMES data is high enough) the difference between the data and calculation at $0.2 < z < 0.5$ is less than 25%. This means that the HERMES data on yields agree with the EMC data which are in accordance with the MC simulations done with the default parameters. It follows from the above discussion that the HERMES data contradicts presumably with the yields obtained in [8].

Fig. 13 shows a comparison of the HERMES data with the theoretical predictions. The dashed histogram has been calculated with the fragmentation functions proposed by Binnewies, Kniehl, Kramer

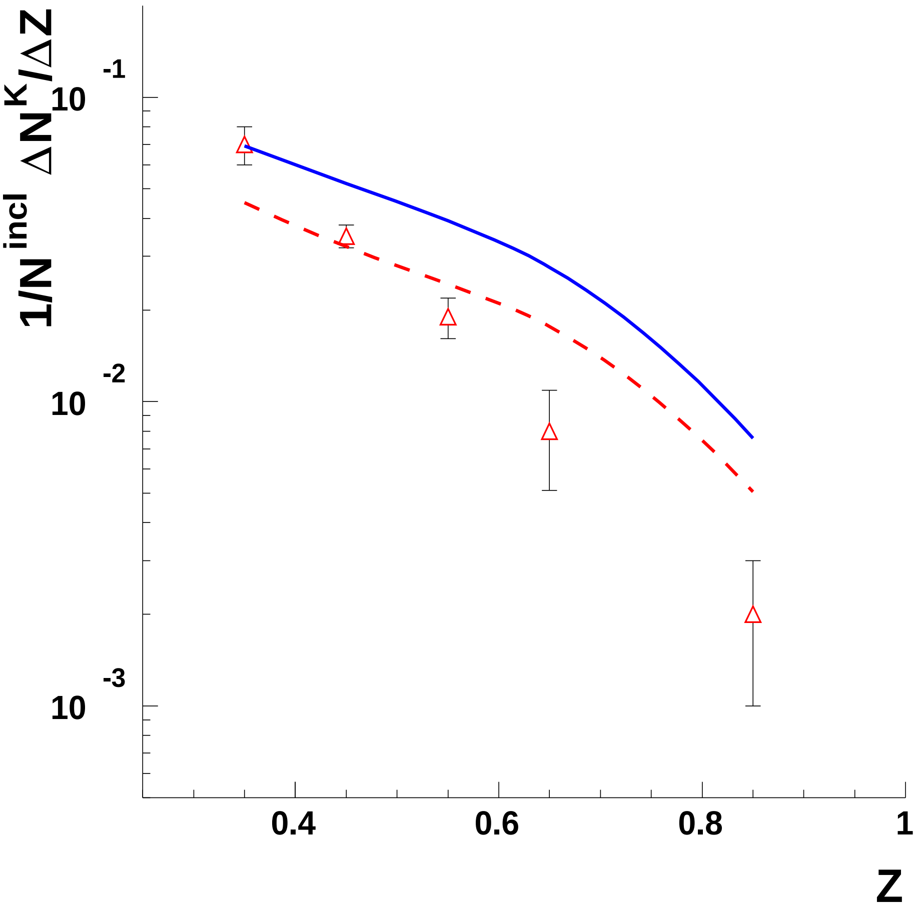

Figure 12: Comparison of relative yields of K_S^0 on proton with Monte Carlo calculations. Experimental data : $\triangle$ - Cornell Univ. ($e+p$, p_{lab}=11.5 Gev/c) [8]. Solid and dashed histograms - MC calculations with default and Cornell parameters, respectively.

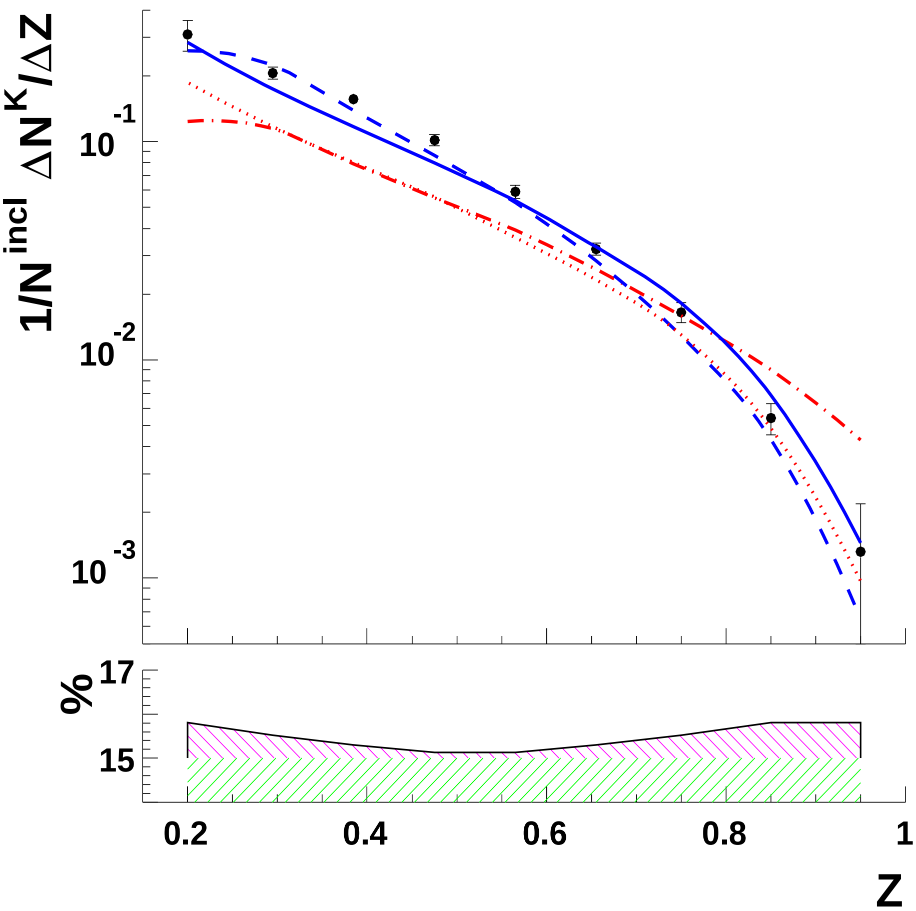

Figure 13: Comparison of relative yields of K_S^0 on proton with calculations. Experimental data : • - HERMES ($Q^2 > 1$ (GeV/c)^2). Shaded area in down part of Figure shows fractional systematic errors. Solid and dotted histograms - MC calculations with default and Cornell parameters, respectively. Dashed and dash-dotted histograms obtained with fragmentation functions [11] and [12], respectively. For last two cases parton distributions [13] have been used.

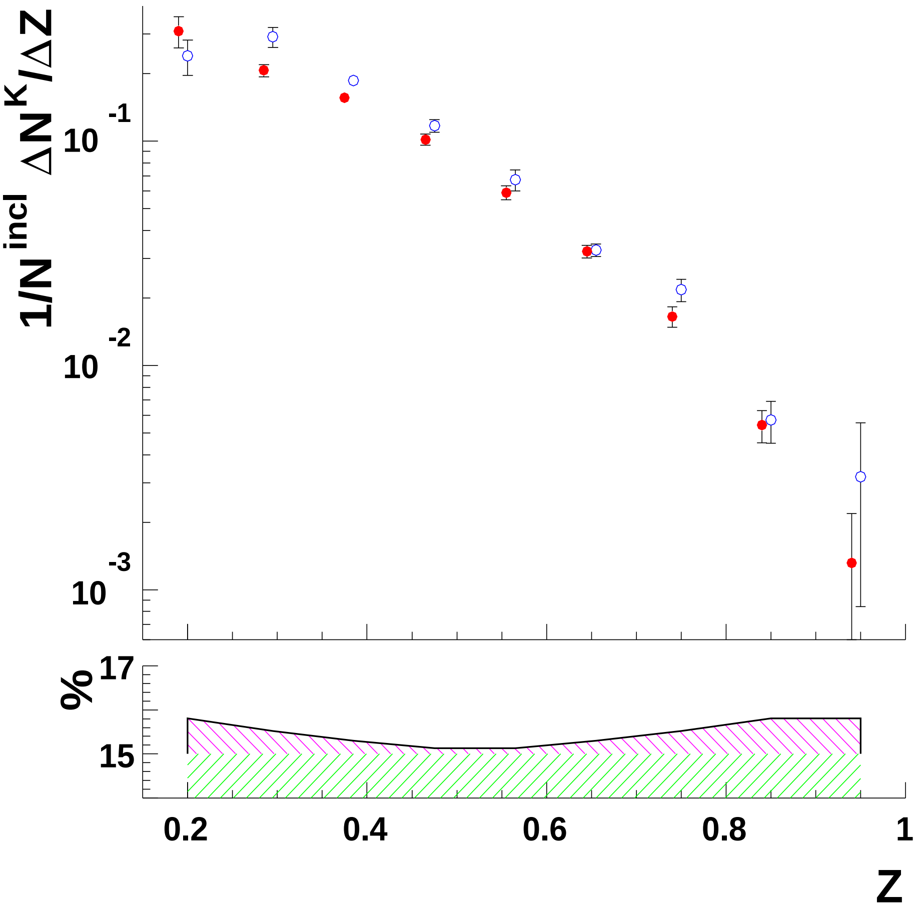

Figure 14: Experimental yields on hydrogen and deuterium versus z. Experimental data : HERMES ($Q^2 > 1$ (GeV/c)^2) $\bullet$ - proton target, $\circ$ - deuteron target. Shaded area in down part of Figure shows fractional systematic errors.

[11] ($\chi^2/N_{d.f.} = 2.99$) and the dash-dotted histogram has been computed with the fragmentation functions by Kaidalov and Piskunova [12] ($\chi^2/N_{d.f.} = 33.03$). For the both calculations the leading order parton distributions [13] have been used. The fragmentation functions [11] have accumulated the experimental information obtained in K^+ and K^- production in the e^+e^--annihilation. To get the fragmentation function for K_S^0 we have used the relations

$$D_u^{K_S^0}(z) = D_{\bar{u}}^{K_S^0}(z) = \frac{1}{2}[D_d^{K^+}(z) + D_d^{K^-}(z)] \; ,$$
$$D_d^{K_S^0}(z) = D_{\bar{d}}^{K_S^0}(z) = \frac{1}{2}[D_u^{K^+}(z) + D_u^{K^-}(z)] \qquad (15)$$

which follow from the isospin and charge conjugation invariance of the strong interaction. Besides it has been assumed in [11] that the valence quark fragmentation functions obey the relation

$$D_s^{K_S^0}(z) = D_{\bar{s}}^{K_S^0}(z) = D_d^{K_S^0}(z) \; . \qquad (16)$$

We see from Fig. 13 that the fragmentation functions [11] describe the HERMES data even better than the MC simulation which makes use of the LUND model for the quark fragmentation ($\chi^2/N_{d.f.} = 6.03$). The fragmentation functions [12] have been extracted from the data on kaon production in hadron-hadron collisions at intermediate energies. We see that they describe the HERMES data worse than the fragmentation functions [11].

A z-dependence of the relative yields per nucleon on the hydrogen and deuterium targets obtained in the present report is shown in Fig. 14 radiation corrections being taken into account. We see that the yields coincide within the statistical uncertainties everywhere except the region $0.25 < z < 0.45$.

A comparison of the $P_\perp^2$-dependence of the relative yields of K_S^0 on the proton obtained in the HERMES experiment with the Cornell university group data is presented in Fig. 15. The radiation corrections have not been taken into account in the presented data. The

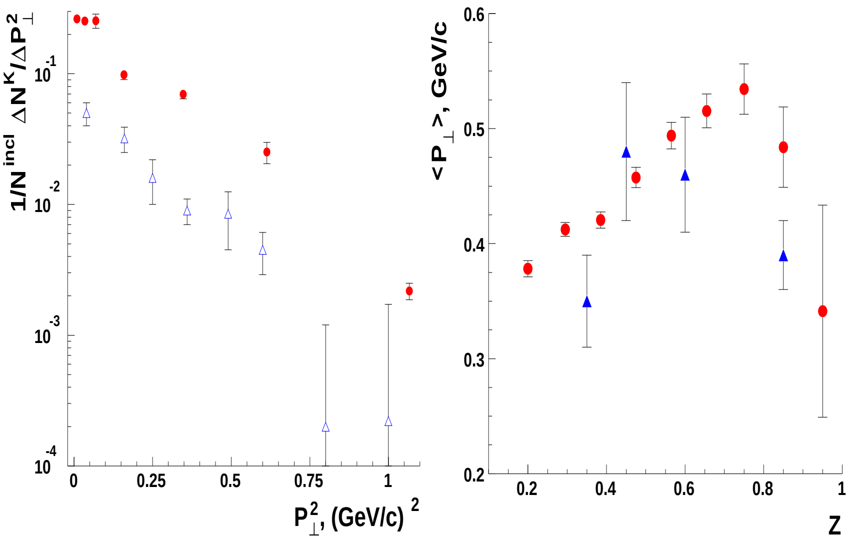

Figure 15: Dependence on $P_\perp^2$ of experimental yields on hydrogen. Experimental data :• - HERMES ($Q^2 > 1$ (GeV/c)^2), △- Cornell data [8]. Right part of Figure shows mean value of $P_\perp$ versus z.

---

left part of the Figure shows that the two data have different normalization factors but values of the slope parameter do not disagree. The right part of Fig. 15 shows a mean value of the K_S^0 transverse momentum $< P_\perp >$ for nine z-bins. We see that the z-dependence of $< P_\perp >$ obtained in the present report does not contradict with the Cornell university group data but statistical uncertainties of the HERMES data is much higher than the data [8].

A comparison of a $P_\perp^2$-dependence of the relative yields of K_S^0 on the hydrogen and deuterium targets (the HERMES data only) with the MC calculations done with the default parameters is shown in Fig. 16. The radiation corrections have been taken into consideration for the experimental data. It is easy to see from the left part of the Figure that the $P_\perp^2$-dependences for both targets are practically identical. One can see also that a difference between the MC calculation and the experimental distributions is less than 35%. Nevertheless since a typical statistical uncertainty of the HERMES data is about 10% the difference under discussion is significant.

Table 5: $< P_\perp >$ for K_s^0 as function z.

$< z >$	$< P_\perp >$
0.2	0.378±0.007
0.295	0.412±0.006
0.385	0.421±0.007
0.475	0.458±0.009
0.565	0.49±0.01
0.655	0.52±0.01
0.75	0.53±0.02
0.85	0.48±0.03
0.95	0.34±0.09

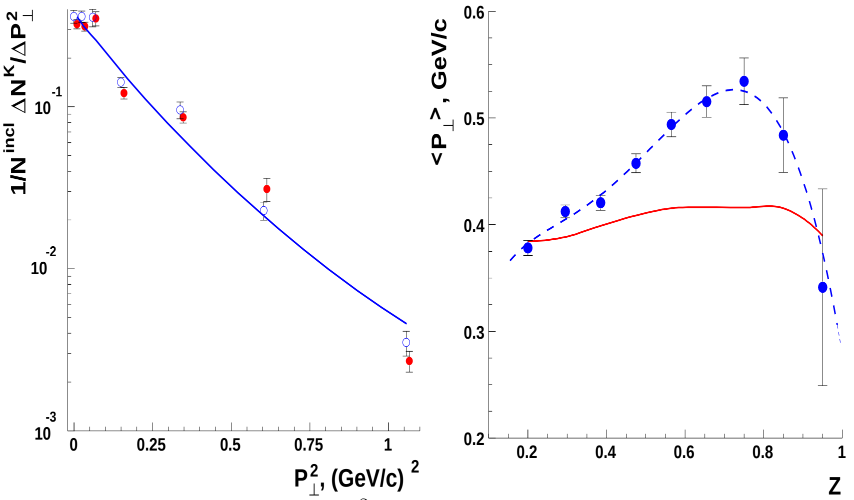

Figure 16: Comparison of $P_\perp^2$-dependence of experimental yields on hydrogen and deuterium with MC calculations. Experimental data : HERMES ($Q^2 > 1$ (GeV/c)^2) • - proton target, ∘ - deuteron target. Right part of Figure shows mean value of $P_\perp$ versus z. Lines show results of MC simulations.

The right part of Fig. 16 shows a comparison of the experimental z-dependence of $< P_\perp >$ with the behaviour of the mean value of the K_S^0 transverse momentum computed with the aid of the MC programs. We see that these dependences are very different. We have approximated the z-dependence of $< P_\perp >$ for the joint data (for the hydrogen and deuterium targets) with the function

$$< P_\perp >= \sqrt{z}(g_0 + g_1 z + g_2 z^2 + g_3 z^3) \tag{17}$$

with $\chi^2/N_{d.f.} = 0.8$ and found the parameters equal to $g_0 = 1.34 \pm 0.03$, $g_1 = -3.5 \pm 0.1$, $g_2 = 6.2 \pm 0.2$, $g_3 = -3.7 \pm 0.2$. We see that the obtained experimental data is not described well by the MC programs. Hence the HERMES data can be used to get improved parameters of the MC generators.

7 Fragmentation functions

One can get the relation for the fragmentation functions $D_u^{K_S^0}(z)$ and $D_d^{K_S^0}(z)$ valid in the quark parton model

$$\begin{aligned} D_u^{K_S^0}(z) &= \frac{1}{8}\frac{(5-8\alpha)Y_D^K + 3Y_H^K}{1-\alpha} + N_u^K(x,Q^2,z) \\ D_d^{K_S^0}(z) &= \frac{1}{2}\frac{(5-2\alpha)Y_D^K - 3Y_H^K}{1-\alpha} + N_d^K(x,Q^2,z) \end{aligned} \tag{18}$$

where α denotes a half of the ratio of the DIS structure functions $F_1(x,Q^2)$ on the deuteron and proton $\alpha = F_1^D(x,Q^2)/[2F_1^p(x,Q^2)]$ and Y_D^K and Y_H^K are relative yields of K_S^0 on the deuterium and hydrogen target, respectively. The expressions for N_u^K and N_d^K are

$$\begin{aligned} N_u^K &= \frac{1}{8}(5G_1 + 3G_2)\ , \\ N_d^K &= \frac{1}{2}(5G_1 - 3G_2) \end{aligned} \tag{19}$$

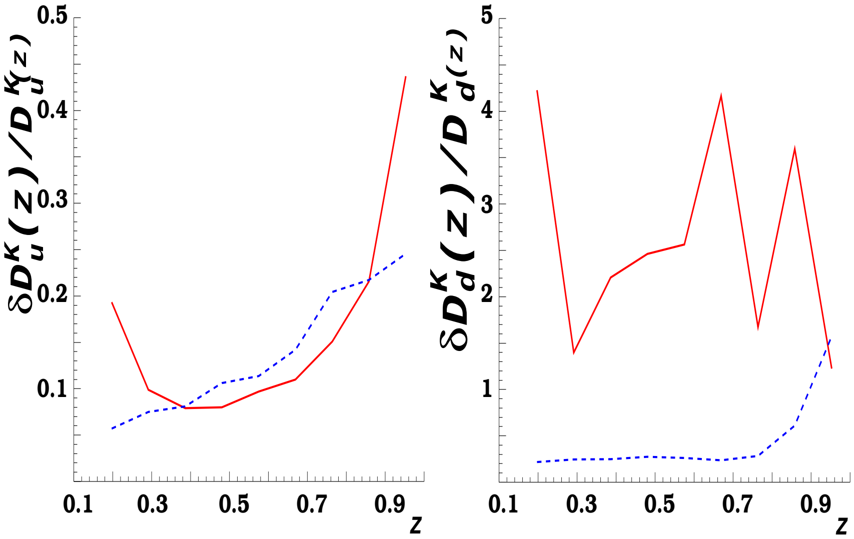

Figure 17: Uncertainties of fragmentation function $D_u^{K_S^0}(z)$ and $D_d^{K_S^0}(z)$. Dashed curves present fractional systematic uncertainties due to neglect with terms N_u^K and N_d^K in (18). Fractional statistical errors are shown by solid lines.

---

where

$$
\begin{aligned}
G_1 = & \{[4(D_u^K - D_{\bar{u}}^K) + (D_d^K - D_{\bar{d}}^K)](\bar{u} + \bar{d}) \\
& -s[2(D_s^K + D_{\bar{s}}^K) - \frac{4}{5}(4D_u^K + D_d^K)]\} \\
& /\{5(u_v + d_v) + 10(\bar{u} + \bar{d}) + 4s\} \\
G_2 = & \frac{[4(D_u^K - D_{\bar{u}}^K) - (D_d^K - D_{\bar{d}}^K)](\bar{u} - \bar{d})}{3(u_v - d_v) + 6(\bar{u} - \bar{d})}. \qquad (20)
\end{aligned}
$$

We have omitted in (20) the dependence of the fragmentation functions $D_q^K(z)$ and the quark distributions $q(x)$ on z and x, respectively.

If one neglects the second terms in relations (18) one gets the approximate formulae for $D_u^{K_S^0}(z)$ and $D_d^{K_S^0}(z)$ which express the fragmentation functions through α and the experimental yields of K_S^0 on the hydrogen and deuterium. To get better statistic accuracy one should sum registered events over experimental ranges of Q^2 and y. The neglect with N_u^K and N_d^K leads to the systematic uncertainty of the fragmentation functions $D_u^{K_S^0}(z)$ and $D_d^{K_S^0}(z)$ obtained from relations (18). It is easy to see that $N_u^K \ll D_u^{K_S^0}$ and $N_d^K \ll D_d^{K_S^0}$ for the HERMES kinematic regions. Indeed, G_1, G_2 in (20) are proportional to the small parameters δ_1, δ_2, δ_3 where

$$\delta_1 = \frac{5[\bar{u}(x) + \bar{d}(x)]}{5[u_v(x) + d_v(x)] + 10[\bar{u}(x) + \bar{d}(x)] + 4s(x)}\,,$$

$$\delta_2 = \frac{4s(x)}{5[u_v(x) + d_v(x)] + 10[\bar{u}(x) + \bar{d}(x)] + 4s(x)}\,,$$

$$\delta_3 = \frac{3[\bar{u}(x) - \bar{d}(x)]}{3[u_v(x) - d_v(x)] + 6[\bar{u}(x) - \bar{d}(x)]} \qquad (21)$$

since the dominant contributions to the yields come from the valence quarks for the HERMES kinematic regions. Besides, the ratios $G_1/D_q^{K_S^0}$, $G_2/D_q^{K_S^0}$ $(q = u,\ d)$ in (20) contain small factors $\epsilon_1 = |[D_u^{K_S^0} - D_{\bar{u}}^{K_S^0}]/D_q^{K_S^0}|$, $\epsilon_2 = |[D_d^{K_S^0} - D_{\bar{d}}^{K_S^0}]/D_q^{K_S^0}|$. A smallness of ϵ_1 and ϵ_2 is related to the fact that probabilities to find a quark and antiquark of any flavour in K_S^0 are equal to each other (we ignore the CP-violation terms). We do not put $\epsilon_1 = 0$ and $\epsilon_2 = 0$ as it has been done in the fragmentation functions proposed in [11] in accordance with (15), (16).

We can estimate values of N_u^K and N_d^K averaged over the HERMES experimental ranges of Q^2 and y using the MC simulation. Figure 17 (left) shows that the fractional systematic uncertainty of $D_u^{K_S^0}(z)$ due to the neglect with N_u^K in (18) is less than 25%. We see that it is comparable with the statistical uncertainty of the fragmentation function. It is easy to see from Figure 17 (right) that the

Table 6: Dependence of fragmentation functions D_u^K on z.

$< z >$	D_u^K
0.2	$0.39^{\pm 0.08}_{\pm 0.07}$
0.295	$0.15^{\pm 0.02}_{\pm 0.03}$
0.385	$0.120^{\pm 0.007}_{\pm 0.02}$
0.475	$0.079^{\pm 0.006}_{\pm 0.01}$
0.565	$0.046^{\pm 0.004}_{\pm 0.009}$
0.655	$0.028^{\pm 0.002}_{\pm 0.006}$
0.75	$0.014^{\pm 0.002}_{\pm 0.004}$
0.85	$0.0057^{\pm 0.001}_{\pm 0.002}$
0.95	$0.0010^{\pm 0.0002}_{\pm 0.0003}$

fractional systematic uncertainty of $D_d^{K_S^0}(z)$ owing to the neglect with N_d^K is less than 30% for $z < 0.8$ which is an upper limit of the accuracy of $D_d^{K_S^0}(z)$ which can be achieved with the applied method. But the statistical uncertainty is greater than 100% which makes meaningless an extraction of the fragmentation function $D_d^{K_S^0}(z)$ for the existing number of experimental events.

Our final result for $D_u^{K_S^0}(z)$ and the comparison of the obtained fragmentation function with theoretical predictions is shown in Fig. 18. All the systematic uncertainties are added in quadrature. They are presented in the down part of the Figure as the shadowed area. We see that the best agreement ($\chi^2/N_{d.f.} = 1.1$) of the obtained fragmentation function $D_u^{K_S^0}(z)$ is with the fragmentation function by Binnewies, Kniehl, Kramer [11]. We see also that the MC simulation with the default parameters does not contradict to the HERMES data ($\chi^2/N_{d.f.} = 3.68$). The calculation performed with the fragmentation function taken from [12] and the MC simulation with the parameters proposed by the Cornell university

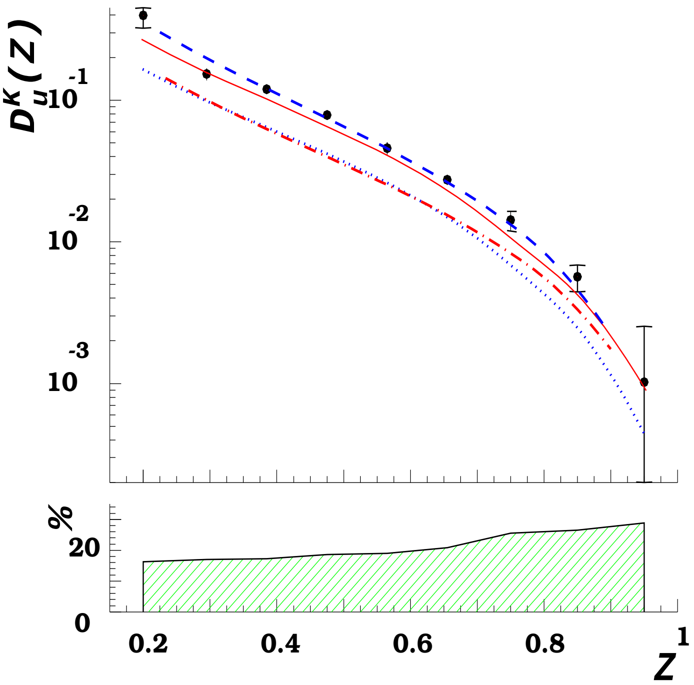

Figure 18: Dependence of fragmentation functions on z. Solid and dotted lines - MC calculations within framework of LUND model, with default parameters and parameters found in [8], respectively. Dashed and dash-dotted curves show fragmentation functions taken from [11] and [12], respectively. Shaded band in bottom part of Figure shows fractional systematic uncertainty.

group disagree with the obtained experimental fragmentation function ($\chi^2/N_{d.f.} = 21.8,\ \chi^2/N_{d.f.} = 21.3$).

8 Conclusion

The relative yields of the K_S^0-production in SIDIS on the hydrogen and deuterium targets based on the analysis of the HERMES 1996, 1997 data are obtained with statistical errors ∼10%. The most important among the systematic uncertainties of the yields is the uncertainty due to the azimuthal dependence both of the detector efficiency and the cross section of the K^0_S-production (15%). Two unfolding methods [1], [2] have been used for the present analysis. They give the results being in an excellent agreement. The relative yields of K^0_S on the proton obtained in the present report are in a reasonable agreement with the EMC data [7] and disagree presumably with the FNAL [9] and the Cornell university group [8] data. The yields obtained in the HERMES experiment have higher statistical accuracy than those of [7], [9], [8]. The number of events collected by the HERMES detector permits to obtain the fragmentation function $D_u^K(z)$ with the statistical accuracy $\sim 7-20\%$. The obtained fragmentation function is in agreement both with the prediction of the LUND model and with the fragmentation function found in [11] and disagrees with the fragmentation functions proposed in [12]. The radiation corrections to the relative yields and the fragmentation function are taken into account with the aid of the POLRAD2 program [10]. The systematic uncertainty of the fragmentation function $D_u^{K^0_S}(z)$ due to the neglect with the term N_u in (18) is shown to be of the same order of magnitude as the statistical errors. The $P_\perp^2$-dependence of the experimental yields on ${}^1H$ and ${}^2H$ agrees with the MC calculations within 35% accuracy but gives unsatisfactory $\chi^2/N_{d.f.} = 4.2$. The experimental z-dependence of the mean value of $P_\perp$ is in contradiction with the MC calculations.

References

[1] V. Blobel, CERN Proceedings , CERN 85-09, p. 88-127, Geneva, 1985.

[2] G. D'Agostini, *Nucl. Instr. Meth.* **A362** (1995) 487.

[3] A. A. Jgoun, the HERMES internal report 99002.

[4] A. A. Jgoun, S. I. Manayenkov, the HERMES internal report 99007.

[5] G. Ingelman, A. Edin, J. Rathsman, "LEPTO 6.5 - A Monte Carlo Generator for Deep Inelastic Lepton-Nucleon Scattering"; preprint DESY 96-057
T. Sjöstrand, JETSET 7.4 , *Comp. Phys. Comm.* **82** (1994)

[6] C. Caso et al., *Phys. Rev.* **C3** (1998) 1.
R. G. Hicks et al., *Phys. Rev. Lett.* **45** (1980) 765.

[7] M. Arneodo, A. Arvidson, J. J. Aubert et al., *Phys. Lett.* **B145** (1984) 156

[8] I. Cohen, R. Erickson, F. Messing et al., *Phys. Rev.* **40** (1978) 1614.

[9] R. G. Hicks et al., *Phys. Rev.* **B45** (1980) 765.

[10] I. Akushevich, A. Ilyichev, N. Shumeiko, A. Soroko and A. Tolkachev hep-ph/9706516 26 Jun 1997

[11] J. Binnewies, B. A. Kniehl, G. Kramer. *Z. Phys.***C65** (1995) 471.

[12] A. B. Kaidalov, O. I. Piskunova, *Sov. J. Nucl. Phys.***41** (1985) 816.

[13] Glueck, Reya, Vogt, *Z. Phys.* **C67** (1995) 433.